JACS
JOURNAL OF THE AMERICAN CHEMICAL SOCIETY
Communication
pubs.acs.org/JACS

Ultrathin Pt–Cu Nanosheets and Nanocones

Faisal Saleem, Zhicheng Zhang, Biao Xu, Xiaobin Xu, Peilei He, and Xun Wang*

Department of Chemistry, Tsinghua University, Beijing 100084, People's Republic of China

Supporting Information

ABSTRACT: In this work, we have successfully synthesized free-standing ultrathin Pt–Cu alloy nanosheets of 4–6 atom thickness with tunable lateral size from 10 to 50 nm. The nanosheets with diameters >20 nm can be converted into nanocones in a controllable way. These nanosheets and nanocones exhibit excellent electrocatalytic activities for the oxidation of ethanol in comparison to commercial Pt black and Pt/C catalysts.

Noble-metal-based alloy nanocrystals play a very important role as catalysts.[1−4] By combining less expensive transition metals with noble metals, forming an alloy will not only reduce the amount of expensive noble metals but also improve the overall performance due to possible synergetic effects.[5,6] Latest research has shown that in addition to the composition and arrangement of atoms in nanomaterials, crystal plane[7] and dimensionality[8] also play a vital role in determining their fundamental properties. Especially 2D nanostructures with atomic thickness may expose specific crystal planes to the largest extent so that they may show further enhanced catalytic properties. Apart from graphene and related materials,[9,10] there have been substantial research efforts to synthesize free-standing 2D nanocrystals of various layered and nonlayered materials, including metal oxides[11−14] and metal chalcogenides;[15−18] a few examples of pure metal nanosheets, e.g., Pd,[19] Au,[20] and Ag,[21] have also been reported. However, the synthesis of transition metal alloy nanosheets remains a great challenge. For the first time, we have synthesized high-purity Pt–Cu alloy ultrathin nanosheets with tunable sizes from 8 to 50 nm. Interestingly, the nanosheets with diameters >20 nm can be converted into nanocones in a controllable way by a rolling process. Previously, it was believed that only layered 2D nanomaterials such as metal hydroxides and chalcogenides could roll up;[22,23] likewise, palladium nanosheets could fold up only by using ladder polysilane as a template.[24]

Direct ethanol fuel cells (DEFC) have gained great attention due to the distinct advantages of ethanol fuel: easy availability, abundance, low cost, nontoxicity, high energy density, safety for storage and transportation in liquid form, etc. Transition metals such as platinum[25] and their alloys[26,27] are used as effective catalysts for DEFC; their catalytic efficiency depends on their size, shape, and composition. In this paper, nanocones show electrocatalytic activity toward ethanol almost 22 times higher than that of Pt black and 14 times that of Pt/C, due to their unique structure with a hollow interior. Similarly, our nanosheets also showed 14 and 9 times higher activity than Pt black and Pt/C, respectively.

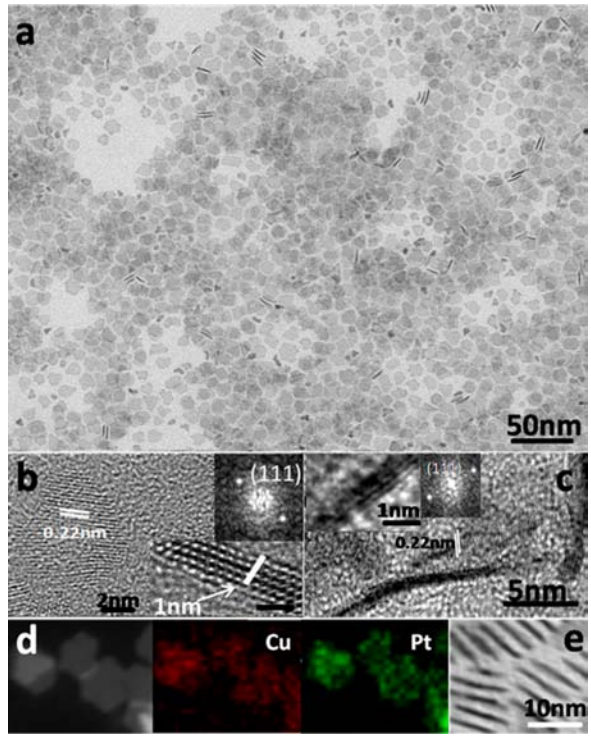

Figure 1. Characterization of Pt–Cu nanosheets: (a) TEM image of nanosheets with a lateral average size of 10 nm; (b) HRTEM image of nanosheets with a lateral average size of 10 nm (insets show the corresponding FFT pattern and thickness of the nanosheet); (c) HRTEM image of nanosheets with lateral size of 20 nm (vertical on TEM grid) with a slight curve (insets show the corresponding FFT pattern and thickness of the nanosheet); (d) HAADF image with corresponding spectral mapping of Cu and Pt; (e) vertical nanosheets on TEM grid.

A two-step method has been developed to prepare ultrathin nanosheets and nanocones of Pt–Cu alloys. In the first step, a gel-like material[28,29] was prepared; it was then used to confine the nucleation and subsequent growth process of the alloy nanocrystals in the second step. Similarly nanocones were prepared in a rolling process by just influencing the reaction conditions with a small amount of HCl in the second step.

A detailed characterization of as-prepared ultrathin nanosheets and nanocones is shown in Figures 1–3. A typical transmission electron microscope (TEM) image shows that samples consist of nanosheets with average lateral lengths of 10 nm (Figure 1a). HRTEM images show that the visible lattice fringes correspond

Received: October 4, 2013
Published: November 25, 2013

dx.doi.org/10.1021/ja4101968 | J. Am. Chem. Soc. 2013, 135, 18304–18307

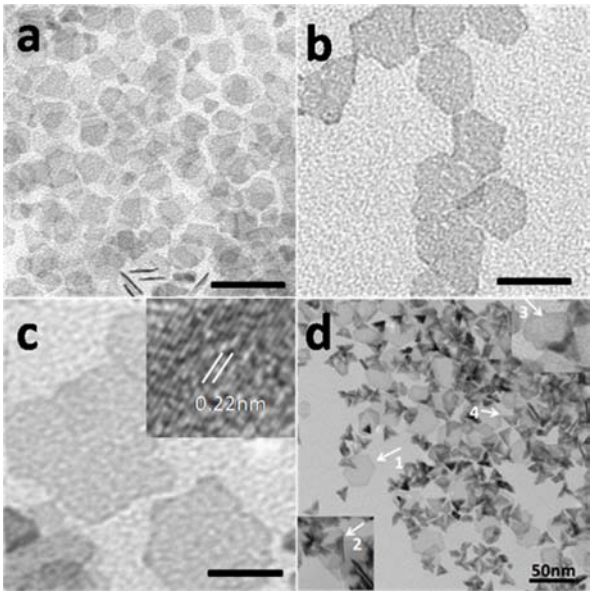

Figure 2. TEM images showing nanosheets of different size on increasing the amount of KI: (a) 10, (b) 20, and (c) 50 nm (inset corresponds to the visible lattice fringes; scale bars 20 nm). (d) TEM image showing nanosheets, half and full curved nanosheets, and nanocones (lower inset shows the magnified image of a nanosheet starting to curve and upper inset shows the magnified image of a nanosheet near to a nanocone shape).

to a spacing of 0.22 nm, which matches well with the expected *d* spacing of the (111) plane of the Pt−Cu alloy (0.218 nm, Figure 1b,c). The thickness of nanosheets ranges from 1.32 to 0.88 nm, directly measured by TEM from nanosheets which were vertical on the TEM grid (Figure S15, Supporting Information), and this is supported by HRTEM on counting the number of atoms in the thickness of the nanosheets: six atoms and four atoms for nanosheets with average lateral sizes of 10 and 20 nm, respectively (insets of Figure 1b,c). A TEM image (Figure 1e) shows the vertical nanosheets on a TEM grid. Atomic force microscopy also determined the thickness of nanosheets with lateral size 50 nm: these nanosheets have a 1.01 nm thickness with fewer than five atoms (Figure S16). Similarly, a TEM image (Figure 3a) shows the purity of nanocones, and the inset shows the HAADF image of nanocones with bright edges which provide strong confirmation of the structures.[30] In Figure 3a, red arrows point out that the nanocones sitting on the tip have a dark point in the center.[31] HRTEM images (Figure 3b,d) show perfect individual nanocones with high crystallinity, and Figure 3d shows tilted angles of a single nanocone. An elemental mapping analysis shows the uniform distribution of both Pt and Cu in all nanocrystals (Figures 1d, 3e, S11). The composition was investigated by energy-dispersive X-ray (EDX) spectroscopy equipped with TEM and supported by inductively coupled plasma optical emission spectrometry (ICP-OES). The consistent results obtained suggest a Cu/Pt molar ratio of ∼2:1 (Figure S12). The X-ray diffraction (XRD) pattern (Figure S13) of the nanocrystals displays characteristic peaks that are in agreement with those of the standard Pt−Cu pattern (JCPDS No. 35-1358). Moreover, no obvious peaks from Pt, Cu, or oxides are detected, confirming the phase purity. XRD data also show evidence for the preferred orientation, with the (111) peak having a higher intensity relative to the (200) and other peaks that would be expected for an anisotropic sample and having the expected face-centered-cubic (fcc) structure type. XRD and EDX

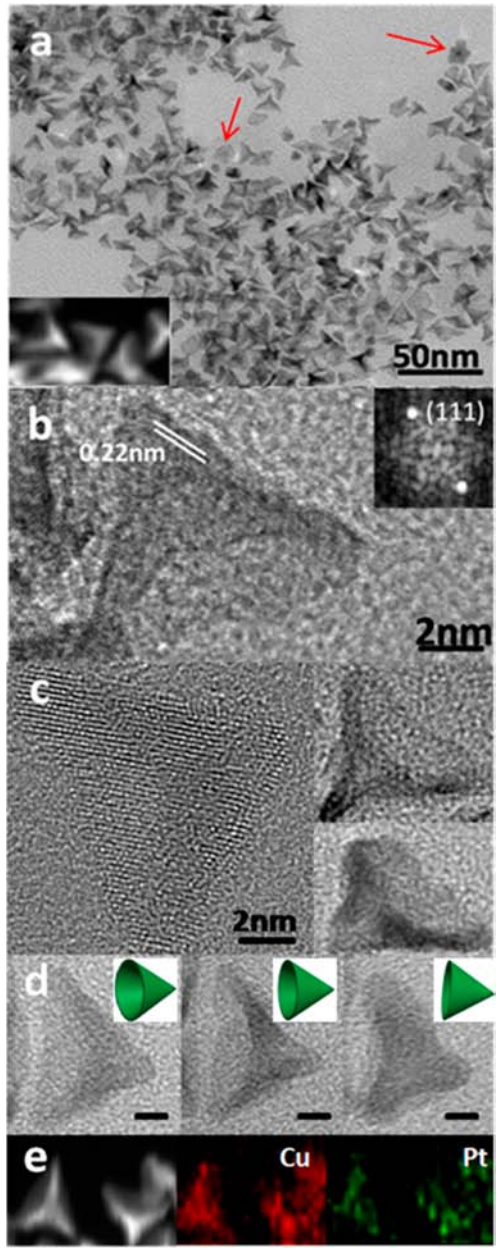

Figure 3. Characterization of Pt−Cu nanocones: (a) TEM image of nanocones (inset shows the HAADF image); (b) HRTEM image of an individual nanocone (inset shows the corresponding FFT pattern); (c) HRTEM images of nanocones; (d) difference orientation of the nanocone (insets are the corresponding crystal model); (e) HAADF image with corresponding spectral mapping of Cu and Pt.

results also show that nanocones are slightly more Pt rich in comparison to Cu.

Potassium iodide played a crucial role in controlling the size of nanosheets and their thickness, while formaldehyde and PVP may act as a reducing reagent and capping reagent, respectively. Increasing the amount of KI from 15 to 40 mg resulted in an increase in the average lateral size of nanosheets from 10 to 50 nm (Figure 2a−c and Scheme 1). At the start when the amount of KI was small, the nanosheets were pure and stable (Figures 1a and 2a,b), but further increasing the amount of KI resulted in the formation of unstable nanosheets, which then started being curved (Figure S3). Keeping in mind these facts, we then investigated the influence of some other parameters such as the

dx.doi.org/10.1021/ja4101968 | *J. Am. Chem. Soc.* 2013, 135, 18304−18307

Scheme 1. Effects of KI and HCl on the Sizes and Rolling Process of Pt−Cu Alloy Nanocrystals

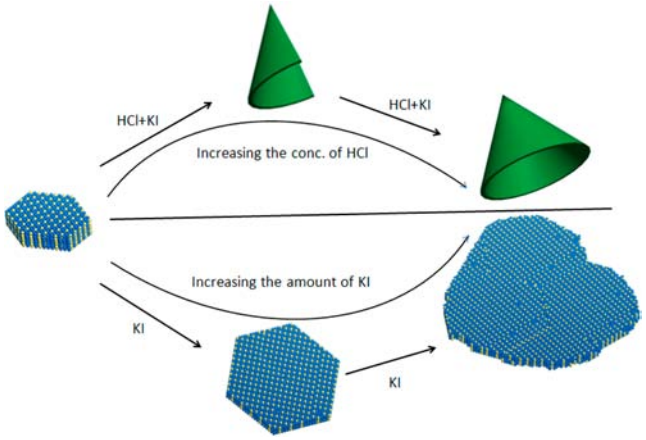

addition of a small concentration of H^+ in the system, which may decrease the reducing capability of HCHO molecules and thus could slow down the reducing rate during the synthesis of our materials.[32] We added 1 μL of HCl in the second step under the same conditions where we already obtained nanosheets 20 nm in size, but this time we got nanosheets and nanocones (half and near-full curved) in the same sample, as indicated by arrows (Figure 2d). In the inset of Figure 2d, we can clearly see a rolling nanosheet, which strongly supports the development of nanocones from nanosheets by a rolling process. Interestingly, further increasing the concentration of HCl (2 μL) resulted in the formation of uniform nanocones (Figure 3a). Again further increasing the concentration of HCl (10 μL) resulted in nanocones with smaller sizes but not as pure; the purity of nanocones further decreased when the amount of HCl was 20 μL (Figure S4). However, the same addition of 2 μL of HCl for the synthesis of nanosheets 50 nm in size (Figure 2c) resulted in the formation of all crumbled nanosheets (Figure S5).

In addition to temperature and capping reagents, the growth of particles greatly depends on the properties of the solution and the interfaces between the particles and the surrounding environment.[33] It has also been found that sizes and surface properties of nuclei may determine their subsequent assembly and growth behavior, and nuclei with smaller sizes may lead to 1D or 2D growth modes.[33] Here a gel-like material increases the viscosity of the solution and may act as a template for the formation of smaller nuclei, which then lead to the 2D growth modes of alloy nanosheets. An FTIR spectrum (Figure S14) of the gel-like material is well matched with those of tris-(hydroxymethyl)aminoethane (Tris) and PVP and also shows a characteristic peak at 1770 cm^{-1} for the carbonyl group of formaldehyde. Similarly, an IR spectrum of the final product shows a peak at 1658 cm^{-1} for the carbonyl group of PVP and one more important peak at 2155 cm^{-1}, which may be from carbon monoxide.[19,34] CO may be produced from the decomposition of formaldehyde[34,35] at high temperature and be captured in the first step; finally, it may play a dual role in the second step as a reducing agent as well as a shape controller. We ran some more reactions to see the effect of Tris, temperature, ratio of metal precursors, and amount of gel under the same conditions where we got 10 nm nanosheets. To see the importance of Tris, we ran the reaction without Tris and got nanosheets with 50% purity. Here, the main function of Tris might be to trap CO, PVP, and formaldehyde by increasing the viscosity of the solution in the first step (Figure S6). Similarly, we varied the temperature, which had a great influence on the morphology of the nanocrystals. At 140 °C, the edges of the nanosheets became thick and particles also appeared in the same sample, and at 150 °C only cubic particles were obtained (Figure S7). To see the effect of different ratios of metal precursors, we ran reactions at 1.3:0.7 and 0.7:1.3 molar ratios of Pt and Cu, respectively. In both cases, we got nanoparticles but no nanosheets (Figure S8). When we ran the reaction by decreasing the amount of gel by half, we got nanosheets with <5% purity, and when we ran reaction with a double amount of gel, we got >80% nanosheets (Figure S9). This clearly showed the importance of the gel. A detailed formation mechaniam, especially the role of the gel in the growth of alloy nanosheets, still deserves investigation; nevertheless, high-purity Pt−Cu nanosheets and nanocones can be reproducibly prepared by using this two-step strategy.

To study the shape effects on the electrochemical properties of as-prepared nanosheets and nanocones, electro-oxidations of ethanol on these Pt−Cu alloy, commercial Pt black, and Pt/C (Alfa Aesar) catalysts were run. Before each test, Pt−Cu alloy nanosheets and nanocones were treated with UV irradiation (wavelength at 185 and 254 nm) for 12 h in air to remove the surfactants.

Figure 4 plots the cyclic voltammogram (CV) curves for the electro-oxidation of ethanol on the Pt−Cu alloy nanosheets and

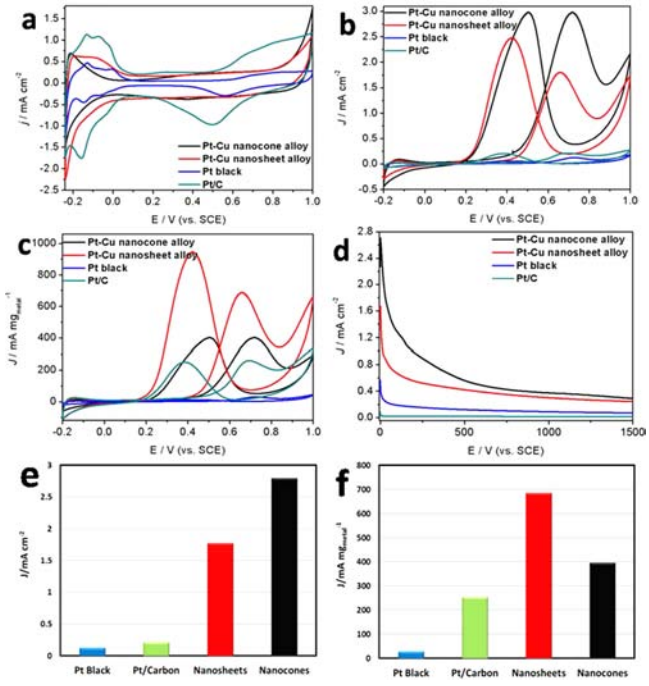

Figure 4. Comparison of electrocatalytic properties of the Pt−Cu nanocone alloy, Pt−Cu nanosheet alloy, Pt black, and Pt/C catalyst: (a) CV curves recorded at room temperature in an N_2-purged 0.5 M H_2SO_4 solution with a sweep rate of 50 mV/s; (b) specific activity, (c) mass activity, and (d) stability (at 0.6 V vs SCE) for these catalysts; (e,f) graphical comparison of specific and mass activities of all catalysts, respectively. Specific and mass activities are given as kinetic current densities (J) normalized with reference to the ECSA and loading amount of metal, respectively. In (a), current densities were normalized with reference to the geometric area of a working electrode (0.07). The ethanol oxidation was recorded in 0.5 M H_2SO_4 + 0.1 M CH_3CH_2OH solution at a scan rate of 50 mV/s.

dx.doi.org/10.1021/ja4101968 | J. Am. Chem. Soc. 2013, 135, 18304−18307

nanocones, commercial Pt black, and Pt/C. The specific current density (J) was normalized to the electrochemically active surface area (ECSA), which was estimated from the hydrogen adsorption/desorption charges using CV data in H_2SO_4 (0.5 M), assuming 210 $\mu C/cm^2$. All of the catalysts showed the characteristic peaks for pure Pt in the forward and backward scans. Furthermore, these Pt−Cu alloy nanocones exhibited enhanced specific activity as compared to commercial Pt black and Pt/C catalysts. It was seen that nanocones exhibited the highest specific activity among these catalysts. The peak current density of ethanol oxidation in the positive potential scan of these nanocones is 2.97 mA cm^{-2}. This value is almost 22 times that of Pt black and 14 times that of Pt/C. Similarly, nanosheets show almost the same result, being 14 and 9 times higher than those of Pt black and Pt/C, respectively (Figure 4b). The enhanced specific electrocatalytic activity for these Pt−Cu alloy nanostructures may be ascribed to the unique geometry together with exposed surfaces, which shows high ECSA values of 62.8 and 20.1 m^2/g for PtCu nanosheets and nanocones, respectively. The mass activity of nanocones is 11 and 1.5 times higher than those of Pt black and Pt/C, respectively, while the mass activity of nanosheets is 19 and 2.7 times higher than those of Pt black and Pt/C, respectively (Figure 4c). The activities in our studies are superior to the reported activities in previous works, under similar test conditions.[25−27,36] To further evaluate the stability of these Pt−Cu alloy nanocones, i−t curves were conducted for 1500 s (Figure 4d). It was seen that these Pt−Cu alloy nanocones possess excellent stability during the electrochemical measurements, in comparison to commercial Pt/C and Pt black catalysts.

In summary, we have succeeded in preparing nanosheets of Pt−Cu transition metal alloys with tunable lateral size and thickness. We also have developed nanocones from these nanosheets by a rolling process in nonlayered nanomaterial, which was previously only observed in layered materials. Furthermore, these nanosheets and nanocones showed exceptional electrochemical oxidation toward ethanol. In the future, this methodology will provide opportunities to prepare and design more valuable nanocrystals. These nanocrystals are expected to remain in focus for fundamental research such as the energy equilibrium among nanosheets, nanocones, and crumbled nanosheets and similarly between smaller and larger nanosheets. These nanocrystals are also expected to provide new opportunities in the field of catalysis and technology development for the preparation of nanodevices.

■ ASSOCIATED CONTENT

Supporting Information

Detailed experimental procedures, additional TEM images, EDS, and XRD, and complete ref 16. This material is available free of charge via the Internet at http://pubs.acs.org.

■ AUTHOR INFORMATION

Corresponding Author

wangxun@mail.tsinghua.edu.cn

Notes

The authors declare no competing financial interest.

■ ACKNOWLEDGMENTS

This work was supported by the NSFC (91127040, 21221062) and the State Key Project of Fundamental Research for Nanoscience and Nanotechnology (2011CB932402).

■ REFERENCES

(1) Lim, B.; Jiang, M.; Camargo, P. H. C.; Cho, E. C.; Tao, J.; Lu, X.; Zhu, Y.; Xia, Y. *Science* **2009**, *324*, 1302.
(2) Wang, D. S.; Li, Y. D. *Adv. Mater.* **2011**, *23*, 1044.
(3) Xia, B. Y.; Wu, H. B.; Wang, X.; Lou, X. W. *J. Am. Chem. Soc.* **2012**, *134*, 13934.
(4) Zhou, S.; Varughese, B.; Eichhorn, B.; Jackson, G.; McIlwrath, K. *Angew. Chem., Int. Ed.* **2005**, *44*, 4539.
(5) Zhu, H. Y.; Zhang, S.; Guo, S. J.; Su, D.; Sun, S. H. *J. Am. Chem. Soc.* **2013**, *135*, 7130.
(6) Wu, J. B.; Qi, L.; You, H. J.; Gross, A.; Li, J.; Yang, H. *J. Am. Chem. Soc.* **2012**, *134*, 11880.
(7) Hu, S.; Wang, X. *Chem. Soc. Rev.* **2013**, *42*, 5577.
(8) Chhowalla, M.; Shin, H. S.; Eda, G.; Li, L.-J.; Loh, K. P.; Zhang, H. *Nat. Chem.* **2013**, *5*, 263.
(9) Novoselov, K. S.; Geim, A. K.; Morozov, S. V.; Jiang, D.; Zhang, Y.; Dubonos, S. V.; Grigorieva, I. V.; Firsov, A. A. *Science* **2004**, *306*, 666.
(10) Watcharotone, S.; Dikin, D. A.; Stankovich, S.; Piner, R.; Jung, I.; Dommett, G. H. B.; Evmenenko, G.; Wu, S.-E.; Chen, S.-F.; Liu, C.-P.; Nguyen, S. T.; Ruoff, R. S. *Nano Lett.* **2007**, *7*, 1888.
(11) Guan, M. L.; Xiao, C.; Zhang, J.; Fan, S. J.; An, R.; Cheng, Q. M.; Xie, J. F.; Zhou, M.; Ye, B. J.; Xie, Y. *J. Am. Chem. Soc.* **2013**, *135*, 10411.
(12) Ida, S.; Shiga, D.; Koinuma, M.; Matsumoto, Y. *J. Am. Chem. Soc.* **2008**, *130*, 14038.
(13) Yan, H.; Yu, Z.; Lu, K.; Zhang, Y.; Wei, Z. *Small* **2011**, *7*, 3472.
(14) Huang, Q.; Hu, S.; Zhuang, J.; Wang, X. *Chem. Eur. J.* **2012**, *18*, 15283.
(15) Min, Y.; Moon, G. D.; Kim, B. S.; Lim, B.; Kim, J.-S.; Kang, C. Y.; Jeong, U. *J. Am. Chem. Soc.* **2012**, *134*, 2872.
(16) Son, J. S.; et al. *Angew. Chem., Int. Ed.* **2009**, *48*, 6861.
(17) Zhao, Y.; Hughes, R. W.; Su, Z.; Zhou, W.; Gregory, D. H. *Angew. Chem., Int. Ed.* **2011**, *50*, 10397.
(18) Li, L.; Chen, Z.; Hu, Y.; Wang, X.; Zhang, T.; Chen, W.; Wang, Q. *J. Am. Chem. Soc.* **2013**, *135*, 1213.
(19) Huang, X.; Tang, S.; Mu, X.; Dai, Y.; Chen, G.; Zhou, Z.; Ruan, F.; Yang, Z.; Zheng, N. *Nat. Nanotechnol.* **2011**, *6*, 28.
(20) Huang, X.; Li, S.; Huang, Y.; Wu, S.; Zhou, X.; Li, S.; Gan, C. L.; Boey, F.; Mirkin, C. A.; Zhang, H. *Nat. Commun.* **2011**, *2*, 292.
(21) Cao, Z.; Fu, H.; Kang, L.; Huang, L.; Zhai, T.; Ma, Y.; Yao, J. *J. Mater. Chem.* **2008**, *18*, 2673.
(22) Liu, X.; Ma, R.; Bando, Y.; Sasaki, T. *Angew. Chem., Int. Ed.* **2010**, *49*, 8253.
(23) Liu, X.; Ma, R.; Bando, Y.; Sasaki, T. *Adv. Mater.* **2012**, *24*, 2148.
(24) Sunada, Y.; Haige, R.; Otsuka, K.; Kyushin, S.; Nagashima, H. *Nat. Commun.* **2013**, *4*, 3014.
(25) Huang, X.; Zhao, Z.; Fan, J.; Tan, Y.; Zheng, N. *J. Am. Chem. Soc.* **2011**, *133*, 4718.
(26) Yang, X.; Yang, Q.; Xu, J.; Lee, C.-S. *J. Mater. Chem.* **2012**, *22*, 8057.
(27) Li, M.; Cullen, D. A.; Sasaki, K.; Marinkovic, N. S.; More, K.; Adzic, R. R. *J. Am. Chem. Soc.* **2012**, *135*, 132.
(28) Xue, P.; Lu, R.; Huang, Y.; Jin, M.; Tan, C.; Bao, C.; Wang, Z.; Zhao, Y. *Langmuir* **2004**, *20*, 6470.
(29) Gao, P.; Zhan, C.; Liu, M. *Langmuir* **2005**, *22*, 775.
(30) Schafer, C.; Gollmer, D. A.; Horrer, A.; Fulmes, J.; Weber-Bargioni, A.; Cabrini, S.; Schuck, P. J.; Kern, D. P.; Fleischer, M. *Nanoscale* **2013**, *5*, 7861.
(31) Zhang, P.; He, J.; Ma, X.; Gong, J.; Nie, Z. *Chem. Commun.* **2013**, *49*, 987.
(32) Yin, A.-X.; Min, X.-Q.; Zhu, W.; Wu, H.-S.; Zhang, Y.-W.; Yan, C.-H. *Chem. Commun.* **2012**, *48*, 543.
(33) Shen, S.; Zhuang, J.; Xu, X.; Nisar, A.; Hu, S.; Wang, X. *Inorg. Chem.* **2009**, *48*, 5117.
(34) Zhang, L.; Chen, D.; Jiang, Z.; Zhang, J.; Xie, S.; Kuang, Q.; Xie, Z.; Zheng, L. *Nano Res.* **2012**, *5*, 181.
(35) Hou, C.; Zhu, J.; Liu, C.; Wang, X.; Kuang, Q.; Zheng, L. *CrystEngComm* **2013**, *15*, 6127.
(36) Ammam, M.; Easton, E. B. *J. Power Sources* **2013**, *222*, 79.